1 February 1822 Compared to 1700-1850

The aim of the first task is to familiarize yourself with the CLIMEAPP and the reanalysis products of the PALEO-RA project. For this purpose, we examine the average temperature in February 1822 in relation to the reference period 1700-1850 (year-round). For that we utilize ModE-RA (use ModE-Sim and ModE-RAclim as well and note the differences). Figure 1 presents a map-shaped global overview with temperature anomalies. An anomaly of up to +10°C can be observed over Scandinavia, extending across Siberia to eastern Russia. This anomaly gradually weakens towards southern Europe and eventually dissipates. Negative anomalies are evident over North America (south-eastern USA -0.5°C), Greenland (-4°C), Africa, and Central Asia (-2°C).

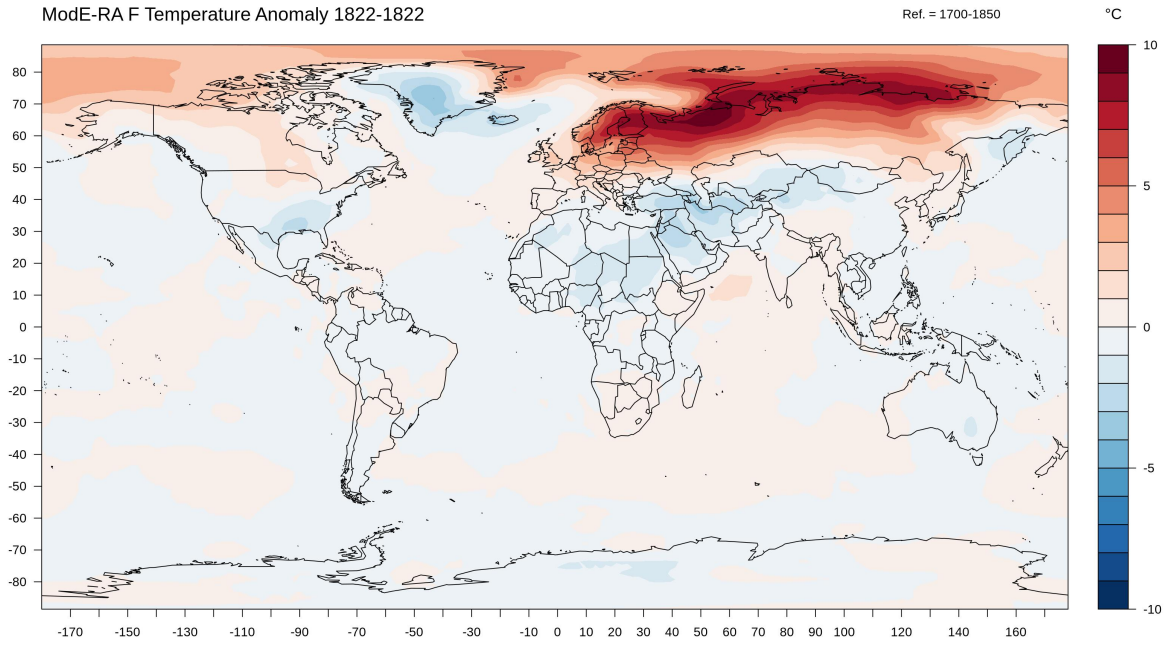

Figure 1: ModE-RA: Map of temperature anomaly of February 1822 compared to the 1700-1850 reference period.

2 Anomalies During Volcanic Years

Since this solution only serves as an example, we focus solely on the years 1815 (Tambora eruption) and 1453 (an unidentified volcanic event supported by sulfur traces in ice cores [see: Sigl et al. 2013]). Our analysis focuses on temperature and precipitation for these two years, as well as on the different reanalyses provided by the PALEO-RA project. Notably, ModE-Sim, being a model without corrections based on observations but incorporating volcanic forcing, is expected to show variations compared to ModE-RA, which includes observation-based corrections. Additionally, ModE-RAclim, where the volcanic forcing has been averaged out, presents another perspective. For analysis of other volcanic years, please proceed exactly the same.

During a volcanic eruption, large amounts of sulfur dioxide are released, which eventually oxidize into sulfate aerosols. This process increases atmospheric optical depth (AOD) and thus scattering, leading to summer cooling (see: Robock et al. 2000). Further, we also can expect a reduction of the African Summer Monsoon due to inhomogeneous cooling of the land and ocean, which decreases the temperature gradient between Europe and Asia and the Pacific and Indian Oceans (see: Zambri et al. 2017).

2.1 Temperature Anomalies

ModE-RA shows a noticeable summer cooling during boreal summer for both the unknown eruption in 1453 and the Tambora eruption in 1815 (Fig. 4 and 5). Regarding the 1453 eruption, ModE-Sim depicts a positive anomaly over southeast Europe of about +0.5°C (Fig. 2), while ModE-RA displays a negative anomaly of about -0.5°C (Fig. 4). This discrepancy arises from corrections based on observations, where observations mainly consist of natural proxies like tree rings. While ModE-Sim provides various plausible climate states under the given boundary conditions and forcings for the respective year within the model physics, ModE-RA represents the "best guess". This accounts for the observed difference. ModE-RAclim also exhibits a boreal summer cooling (Fig. 6), although here the volcanic forcing is averaged out

Figure 5 illustrates the Tambora eruption in 1815 as generated by ModE-RA. The pronounced negative anomaly of about -2°C is notable (often referred to as the 'year without summer'). The disparity between ModE-Sim (Fig. 3) and ModE-RA is not as significant as for the year 1458. This suggests that only a few corrections towards the observations were necessary (utilizing historical documents, temperature measurements, and pressure data). Additionally, ModE-RAclim exhibits a similar pattern to ModE-RA and ModE-Sim (Fig. 7).

2.2 Precipitation Anomalies

To investigate the precipitation anomaly over Africa, we essentially follow the same procedure as for temperature analysis. In Fig. 8 and 9 (ModE-Sim) and Fig. 10 and 11 (ModE-RA), we observe a negative precipitation anomaly over central Africa, corresponding to a reduction in the summer monsoon. The discrepancies between the simulation and the reanalysis are the same as described above.

2.3 Plots: Temperature Anomaly

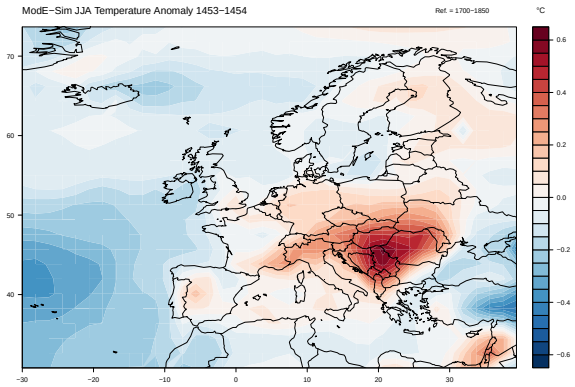

Figure 2: ModE-Sim: Map of temperature anomaly for the JJA Period of the year 1453 (unknown eruption) compared to the 1700-1850 reference period.

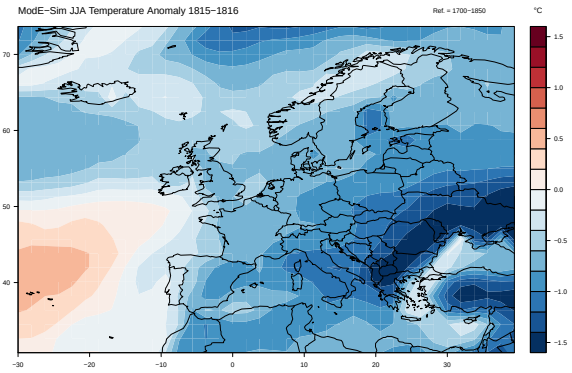

Figure 3: ModE-Sim: Map of temperature anomaly for the JJA Period of the year 1815 (Tambora eruption) compared to the 1700-1850 reference period.

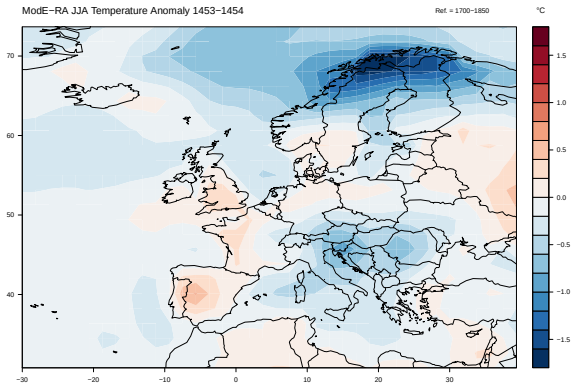

Figure 4: ModE-RA: Map of temperature anomaly for the JJA Period of the year 1453 (unknown eruption) compared to the 1700-1850 reference period.

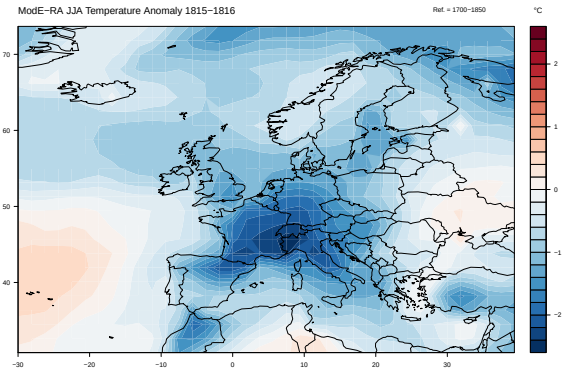

Figure 5: ModE-RA: Map of temperature anomaly for the JJA Period of the year 1815 (Tambora eruption) compared to the 1700-1850 reference period.

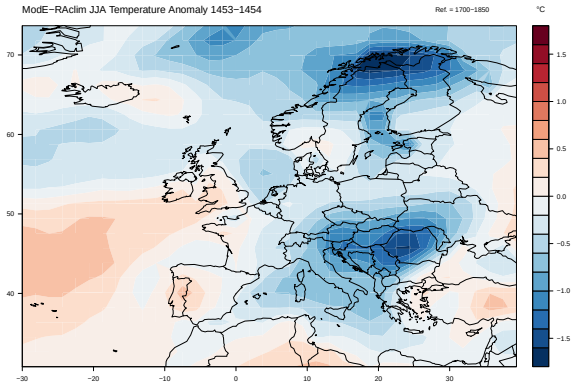

Figure 6: ModE-RAclim: Map of temperature anomaly for the JJA Period of the year 1453 (unknown eruption) compared to the 1700-1850 reference period.

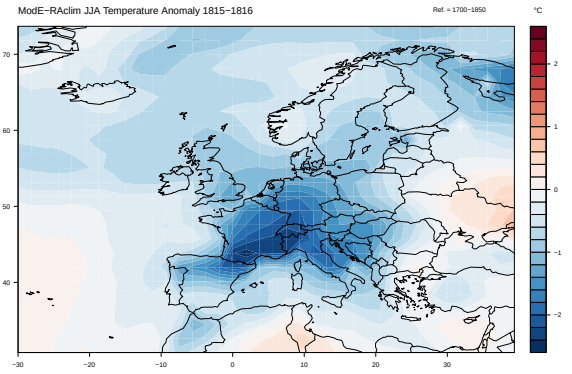

Figure 7: ModE-RA-clim: Map of temperature anomaly for the JJA Period of the year 1815 (Tambora eruption)) compared to the 1700-1850 reference period.

2.4 Plots: Precipitation Anomaly

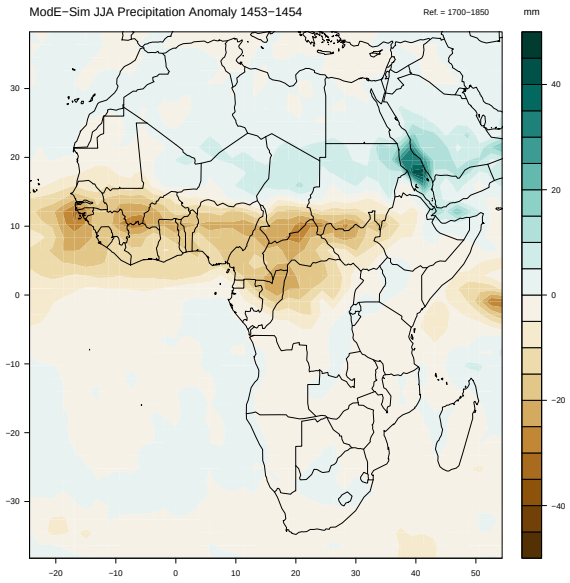

Figure 8: ModE-Sim: Map of precipitation anomaly for the JJA Period of the year 1453 (unknown eruption) compared to the 1700-1850 reference period.

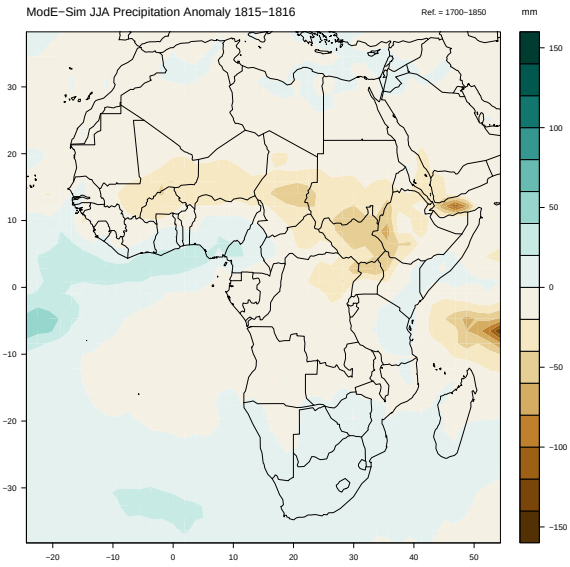

Figure 9: ModE-Sim: Map of precipitation anomaly for the JJA Period of the year 1815 (Tambora eruption) compared to the 1700-1850 reference period.

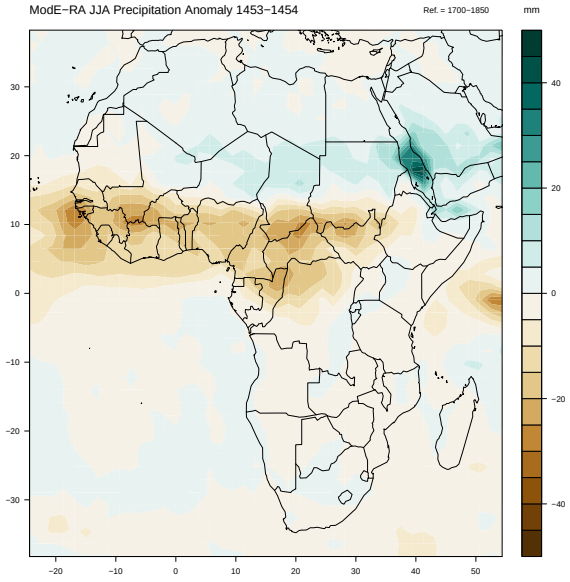

Figure 10: ModE-RA: Map of precipitation anomaly for the JJA Period of the year 1453 (unknown eruption) compared to the 1700-1850 reference period.

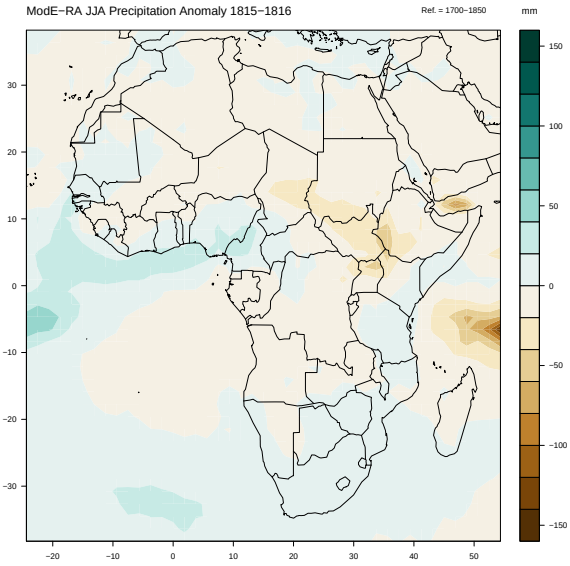

Figure 11: ModE-RA: Map of precipitation anomaly of the JJA Period for the year 1815 (Tambora eruption) compared to the 1700-1850 reference period.

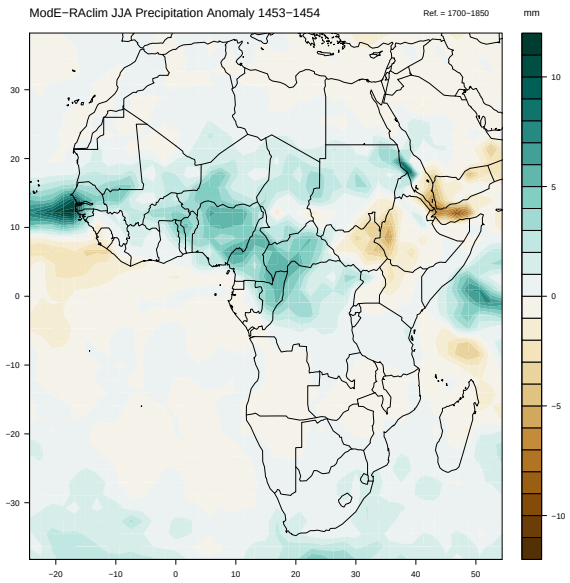

Figure 12: ModE-RAclim: Map of precipitation anomaly of the JJA Period for the year 1453 (unknown eruption) compared to the 1700-1850 reference period.

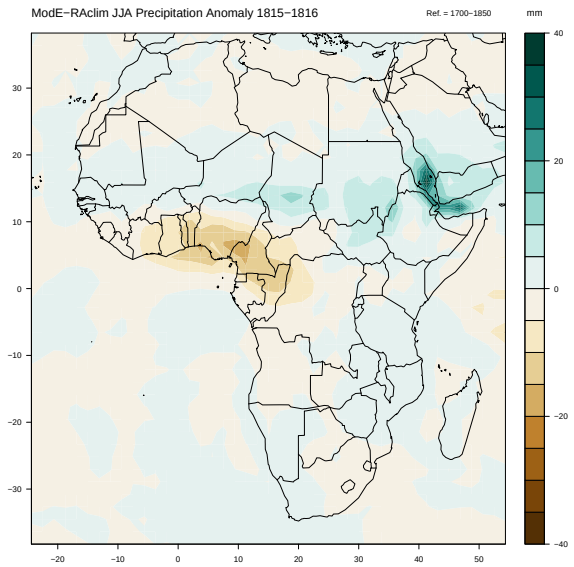

Figure 13: ModE-RAclim: Map of precipitation anomaly for the JJA period of the year 1815 (Tambora eruption) compared to the 1700-1850 reference period.

3 Regression

Here, we utilized the temperature in the Niño 3.4 index field and applied spatial linear regression on the global temperature between 1422 and 2008. Figure 14 illustrates a typical El Niño pattern (warm central Pacific, warmth over Canada and Australia, cold in the southeast of the USA and Indonesia) and La Niña pattern (more or less vice versa to El Niño). For further information, refer to: Climatic Changes Since 1700, Brönnimann et al. 2015, p.113f.

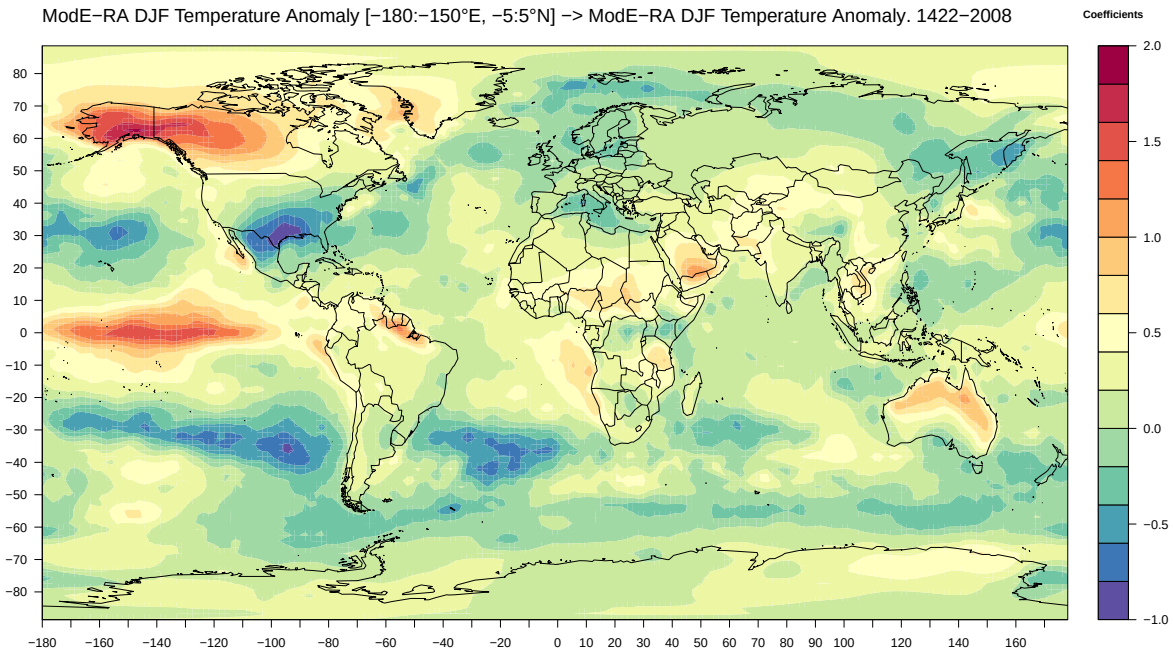

Figure 14: ModE-RA: Map of regression coefficients for the temperature of the Niño 3.4 index and the global temperature.